

---

# GramGAN: Deep 3D Texture Synthesis From 2D Exemplars

---

**Tiziano Portenier**  
ETH Zurich  
Switzerland

**Siavash Bigdeli**  
CSEM  
Switzerland

**Orcun Goksel**  
ETH Zurich  
Switzerland

## Abstract

We present a novel texture synthesis framework, enabling the generation of infinite, high-quality 3D textures given a 2D exemplar image. Inspired by recent advances in natural texture synthesis, we train deep neural models to generate textures by non-linearly combining learned noise frequencies. To achieve a highly realistic output conditioned on an exemplar patch, we propose a novel loss function that combines ideas from both style transfer and generative adversarial networks. In particular, we train the synthesis network to match the Gram matrices of deep features from a discriminator network. In addition, we propose two architectural concepts and an extrapolation strategy that significantly improve generalization performance. In particular, we inject both model input and condition into hidden network layers by learning to scale and bias hidden activations. Quantitative and qualitative evaluations on a diverse set of exemplars motivate our design decisions and show that our system performs superior to previous state of the art. Finally, we conduct a user study that confirms the benefits of our framework.

## 1 Introduction

Texture synthesis is an important field of research with a multitude of applications in both computer vision and graphics. While vision applications mainly focus on texture analysis and understanding, in computer graphics textures are most important in the field of image manipulation and photo-realistic rendering. In this context, applications require synthesis techniques that can generate highly realistic textures. Due to the problem being highly complex, today's applications largely rely on techniques that generate textures based on real photos, which is a time-consuming process that requires expert knowledge. In this work, we present a novel texture synthesis framework that can generate high-quality 3D textures given an exemplar image as input (See Figure 1).

Techniques for texture synthesis can be classified into photogrammetric and procedural techniques. Photogrammetry relies on methods that capture the color appearance of physical objects to obtain (typically several) photos from the target texture. Next, texture mapping algorithms are employed to supply a digital 3D model, usually a polygon mesh, with texture coordinates that define a mapping from 3D surface points to 2D texture pixels. Such photogrammetric approaches yield high-quality textures but rely on time-consuming procedures that require expert knowledge. Moreover, the required projection from 3D to 2D introduces seam and distortion artifacts, for example when texturing spherical objects. Nevertheless, this is still a widely used technique, despite its shortcomings.

An entirely different class of techniques is referred to as *procedural texturing*, where textures are generated by an algorithm instead of relying on acquired data. Ideally the algorithm takes a 3D position as input and computes a texture color value as output, omitting the error-prone projection step entirely. Pioneering work in procedural texturing is the Perlin noise texture model [1], which dates back to 1985. The core idea is to linearly combine noise frequencies, or octaves, to generate different textures. An artist manually adjusts octave weights to obtain a specific look. While this early

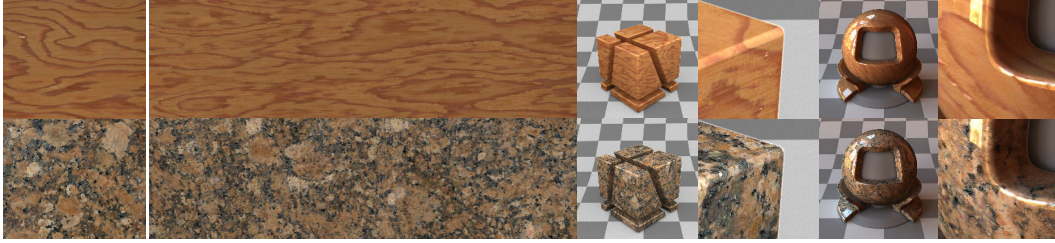


Figure 1: Results produced by our framework. Given an exemplar texture image (left), our model can faithfully resynthesize it infinitely (middle), suitable to texture 3D models (right).

approach conveniently avoids both data acquisition and texture mapping, its applicability to natural textures is rather limited mainly due to the predefined, fixed noise frequencies. Moreover, a user has to manually tweak the parameters in order to obtain a desired look, which is a tedious process.

Recently, several techniques that leverage deep learning have been proposed to train generative models for procedural texture synthesis. Most of these leverage convolutional neural networks (CNNs) to generate texture pixel values as a function of spatially neighboring data. Recent examples in this direction either use generative adversarial networks (GANs) [2] or a style loss [3] to optimize their models. While these CNN-based approaches yield high-quality textures, in practice their application is limited to either 2D textures or very low resolution 3D textures due to the high memory footprint of 3D CNNs. Moreover, an unsolved problem with these techniques is the lack of diversity or rather *stochasticity*, i.e. such models struggle producing diverse results that represent the same texture. Despite attempts to mitigate this problem by explicitly minimizing a diversity term [4], true diversity has not been demonstrated by this approach.

Our work is inspired by the model proposed by Henzler et al. [5], which features both memory efficiency and diversity. The former is achieved by formulating the texture synthesis problem as a point operation parametrized using a multilayer perceptron (MLP), while the latter is achieved by defining the model to be a function of noise frequencies, similarly to Perlin. However, this flexibility comes at the cost of lower image quality and a lack of similarity to the exemplar texture.

We present a point operation model that learns to generate textures as a function of noise frequencies, but we propose a novel loss function and architectural framework, which together improve image quality significantly. Moreover, our proposed network architecture inherently supports an extrapolation technique that improves generalization to unseen textures, that can be substantially different from the training set exemplars. In particular, we make the following contributions: (1) a deep MLP architecture that effectively combines learned noise frequencies; (2) a novel GAN loss inspired by style transfer to achieve both realistic image quality and high similarity to the input exemplar; and (3) a novel extrapolation strategy that significantly improves the results on unseen exemplars.

## 2 Related work

Texture synthesis techniques have a long history in computer vision and graphics. In 1985, Perlin [1] proposed a model to generate stochastic textures by linearly combining frequencies of noise in 2D or 3D. By using different combination weights, various visual appearances can be created. However, due to fixed, isotropic frequencies, the model expressiveness is limited and the space of generated textures is restricted to isotropic textural features, inhibiting anisotropic, e.g. elongated structures. Another major limitation of this model in practice is that the linear weights must be tediously tweaked to obtain an output that matches a desired texture. To overcome this limitation, a desired property of any texture synthesis method is the ability to generate textures that automatically match an exemplar texture at hand. Early works that tackle this problem are patch-based techniques [6–11], where texture exemplars are either padded, inpainted, or reproduced from scratch by considering local neighborhoods in the exemplar image. While these methods can faithfully reproduce a target texture, they are limited to 2D and are computationally expensive. With recent advances in deep learning, a multitude of learned texture synthesis models have been proposed in the vision community. Most such work either optimize a style loss [3], a GAN loss [2], or a hybrid of the two. As our work is closely related to these approaches, we give an overview of the respective methods in the following.

**Texture synthesis using style loss** In their groundbreaking work, Gatys et al. [3] demonstrated that statistical correlations of activations extracted from a pre-trained VGG-19 network [12] encode textural features. In particular, it has been shown that matching the Gram matrices of these deep activations successfully guides the synthesis network to generate samples similar to the target texture. Building upon these insights, several methods have been proposed to improve computation time [13, 14] and diversity [15] of texture generation. All such models are parametrized using CNNs and therefore they do not scale well to 3D textures at acceptable texture resolutions. Moreover, these approaches all work on a single exemplar texture, which implies the need for training an individual model for each target texture. Finally, obtaining true diversity in generated samples is still an unsolved problem with these methods. A big leap forward has been achieved recently by Henzler et al. [5]. They propose a point operation model parametrized as an MLP instead of using CNNs, which enables efficient synthesis of high-resolution 3D textures. Moreover, true diversity is demonstrated thanks to combining noise frequencies directly, similarly to Perlin noise textures. Finally, their model is capable of synthesizing an entire space of textures, rather than a single exemplar, when trained on a set of exemplar textures. However, the resulting texture quality is not yet on par with state of the art CNN models and the synthesized textures are often relatively different from the respective target exemplars. In our work, we also model point operations that combine noise frequencies to efficiently support diverse 3D texture synthesis. However, we show that our novel GAN loss and network architecture significantly improve image quality and similarity to target textures. Moreover, we demonstrate superior generalization performance enabled by our proposed network architecture.

**Texture synthesis using GANs** GANs are another widely used class of models for texture synthesis, by training a CNN generator  $G$  to fool a CNN discriminator  $D$  in an adversarial minimax game [16–19]. Most such approaches learn purely generative models, often trained on individual exemplars. An effective technique to incorporate a user-provided exemplar is conditional GANs [20], as shown by Alanov et al. [21]. Here,  $G$  synthesizes a texture given an exemplar patch as input. To enforce  $G$  to respect its input,  $D$  discriminates the joint distribution of pairs of texture patches. Here, a sample of the generated distribution consists of a condition patch and a synthesized texture, and a sample of the ground truth distribution consists of two random patches coming from the same texture. A more widely used approach to incorporate a conditional input is to extend the generator loss by an additional style loss term [3] using an off-the-shelf feature extractor (VGG) [22–24]. While GAN-based models achieve astonishing texture quality, even surpassing style-loss based techniques [16], the proposed models all rely on CNNs, hindering their applicability to 3D textures due to computational limitations. While we also leverage GANs in our work to obtain high-quality textures, we propose a model based on point operations, suitable for 3D texture synthesis. Moreover, we incorporate ideas from style-loss based techniques to train a conditional GAN without the need of an additional off-the-shelf network, resulting in a unified loss function that is much more efficient than hybrid losses.

### 3 GramGAN

In this section we introduce our framework for 3D texture synthesis from 2D exemplars. At the core of our method is a texture sampler that is modeled as an MLP to efficiently learn to combine learned noise frequencies using a specialized layer architecture (Figure 2). We train this model by optimizing a novel loss function that incorporates concepts from both GANs and style loss approaches to achieve high-quality outputs. In this work we consider two different target applications: (1) learning to synthesize highly realistic textures from a single exemplar (Section 3.1), and (2) learning a texture latent space given a set of many exemplars (Section 3.2). Later in Section 3.3 we propose an efficient strategy for improving the generalization performance.

#### 3.1 Efficient, infinite, and highly realistic 3D textures from a single 2D exemplar

Given an exemplar image of a target texture, in order to learn a model that can generate new, high-quality samples of the target texture in 3D, we train a transformation model and a texture sampler. Our transformation model learns to produce  $n$  noise frequencies, or octaves  $T_i, i \in [0, n - 1]$ , given the 2D exemplar. These frequencies are linear 3D transformations  $T_i: \mathbb{R}^3 \rightarrow \mathbb{R}^3$  defined as  $T_i c = c_i$  that map a spatial 3D coordinate  $c$  to a set of new locations  $\{c_i\}$ , one location for each frequency.

The sampler  $S$  maps the spatial coordinate  $c$  to its RGB texture value. We first compute a noise value  $\eta_i(c)$  for each octave by trilinearly sampling  $n$  3D Gaussian noise tensor instances  $\bar{\eta}_i \sim \mathcal{N}(0, 1)$

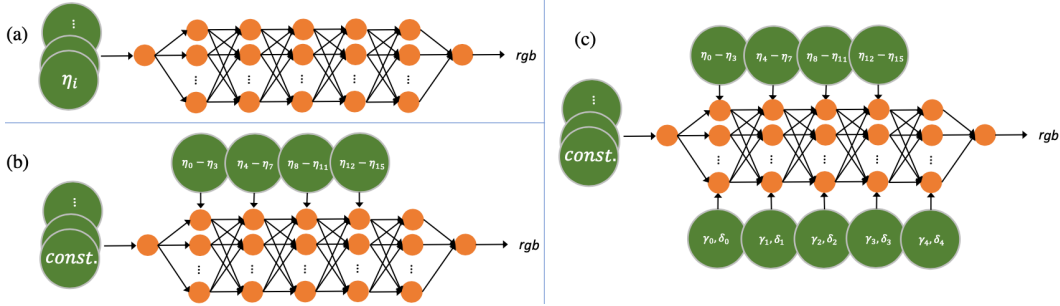


Figure 2: Sampler network models. a) The baseline model, where the noise is inserted at the input layer. b) Our model that combines blocks of noise frequencies at hidden layers (Equation 2). c) Our conditional model that combines the conditional input at each hidden layer (Equation 5).

using the transformed locations  $c_i$ , i.e.,  $\eta_i(c) = \bar{\eta}_i(c_i)$ . This results in an input noise vector  $\eta(c) = (\eta_0(c), \eta_1(c), \dots, \eta_{m-1}(c))$  that is combined by  $S$  to form the final RGB output at location  $c$ :

$$S: \mathbb{R}^n \rightarrow \mathbb{R}^3, \quad S(\eta(c)) = \text{RGB}(c). \quad (1)$$

During training, we simultaneously optimize both the parameters of  $S$  and the  $n \times 3 \times 3$  matrix entries in the transformation model.

We parametrize  $S$  using an MLP with 5 hidden layers, as shown in Figure 2. We find that directly providing the transformed noise  $\eta$  at the input layer yields subpar outputs. Therefore, we propose to inject  $\eta$  into the hidden layers of  $S$  and learn a constant input layer instead. Consider a dense layer defined as  $y = \phi(Wx + b)$ , where  $W$  is the weight matrix,  $b$  is the bias vector,  $x$  is the layer input,  $\phi$  is the activation function, and  $y$  stores the layer activations. We use dense layers of the form:

$$y = \phi(Wx + \psi(\eta) + b) \quad \text{with} \quad \psi(\eta) = A\eta, \quad (2)$$

where  $A$  is a learned  $m \times n$  matrix for a layer with  $m$  hidden units. This concept resembles some similarities to StyleGAN [25], although the input noise has a different role here and network layers of our sampler do not relate to scale in any way. In practice we find it beneficial to force individual layers in  $S$  to specialize on a subset of noise frequencies. This reduces the number of parameters to optimize as well as minimizing the risk of  $S$  ignoring certain frequencies in computation of its output. In particular, we partition the frequencies in equal bins of size  $n/4$  and inject each bin into one hidden layer only. The last hidden layer thus does not receive any noise, which we find to reduce the risk of ignoring other frequencies further, and the dimension of the matrices  $A$  reduces to  $m \times n/4$ .

**Loss function** We optimize the parameters of our model using a GAN loss. However, while our sampler generates 3D textures, our critic  $D$ , parametrized as a standard CNN, discriminates 2D images. In particular, in each training iteration our model synthesizes 2D images by randomly slicing the 3D space. To optimize  $D$ , we use the WGAN-GP loss proposed by Gulrajani et al. [26], i.e.,

$$\mathcal{L}_D = \mathbb{E}[D(f)] - \mathbb{E}[D(r)] + \lambda \mathbb{E}[(\|\nabla_u D(u)\|_2 - 1)^2], \quad (3)$$

where  $f$  is a randomly oriented 2D slice produced by our model,  $r$  is a random patch from the exemplar texture image, and  $u$  is a data point uniformly sampled along the straight line connecting  $r$  and  $f$ . This is a crucial difference to [5], where only axis-aligned slices are sampled during training. To optimize our texture generator  $G$ , we introduce an additional style term  $\mathcal{L}_{\text{style}}$  to the WGAN loss:

$$\mathcal{L}_G = -\alpha \mathbb{E}[D(f)] + \beta \mathcal{L}_{\text{style}} \quad \text{with} \quad \mathcal{L}_{\text{style}} = \frac{1}{L} \sum_{l=0}^{L-1} \frac{1}{4N_l^2 M_l^2} \sum_{i,j} |M_{ij}^l(F(r)) - M_{ij}^l(F(f))|, \quad (4)$$

where  $L$  is the number of hidden layers in a feature extractor network  $F$ ,  $M^l(F(x))$  is the Gram matrix of the activations in layer  $l$  when presenting  $x$  as input to  $F$ ,  $N_l$  is the number of filters in layer  $l$ , and  $M_l$  is the number of pixels in the vectorized activations of layer  $l$ . Note that while previous work on style loss employ pretrained, off-the-shelf feature extractors (typically  $F = \text{VGG-19}$  [3, 13–15, 5, 22–24]), our important difference is that we set  $F = D$ , i.e., we train  $F$  simultaneously with  $G$

in an adversarial manner! This concept has numerous advantages compared to the traditional hybrid approaches based on combinations of GAN and style losses. First, the activations in  $D$  are anyhow computed during GAN training, hence our approach significantly minimizes any computational overhead in loss function evaluation. Second and more importantly, such features explicitly trained for texture discrimination, as we show later, help generate textures of significantly higher quality compared to off-the-shelf features trained on image recognition as in works leveraging VGG. Note that we minimize  $L_1$  distance between Gram matrices in  $\mathcal{L}_{\text{style}}$  as opposed to the  $L_2$  distance commonly used in related work, since we find this to improve the stability of adversarial training.

### 3.2 Learning a latent texture space

While training a distinct texture synthesis model for each target texture is computationally feasible, in practice it is desirable to have a single conditional model that can generate an entire class, or space, of textures. Besides the reduced training computation time, such a model promises generalization capabilities such as interpolation and extrapolation, greatly simplifying the texture generation process from the user perspective. Our goal is to obtain a texture synthesis framework that allows a user to select a 2D image patch of a target texture, and the model can generate new samples of this target texture in 3D without retraining. For this purpose we extend our model proposed in Section 3.1 by an encoder  $E(x) = z$  that maps an input exemplar patch  $x$  to a compact latent representation  $z$ . Similar to Henzler et al. [5], we parametrize  $E$  using a CNN. The idea is now to condition both  $T_i$  and  $S$  on the latent code  $z$ . We therefore train an additional 3-layer MLP  $Q(z) = \{T_i\}$  to map the latent representation  $z$  to a set of noise frequencies  $\{T_i\}$ . Moreover, we extend  $S$  to non-linearly combine noise frequencies given  $z$ , i.e.,  $S(\eta(c)|z) = \text{RGB}(c)|z$ . Instead of presenting the condition  $z$  at the input layer of  $S$ , we find it beneficial to directly manipulate the hidden activations in  $S$  as a function of  $z$  (See Figure 2). Our approach is inspired by attention modules [27] and adaptive instance normalization techniques [28] for CNNs. First, we train a small 3-layer MLP  $f$  to learn a texture style  $w = f(z)$ . Next, each hidden layer  $l$  learns an affine mapping  $g_l(w) = (\gamma, \delta)$  that computes a scale and bias for each unit in the respective layer. The definition from Equation 2 therefore extends to

$$y = \gamma(\phi(Wx + \psi(\eta) + b)) + \delta \quad \text{with} \quad \gamma, \delta \in \mathbb{R}^m. \quad (5)$$

Note that in order to synthesize a texture sample given an input exemplar, a single forward pass through  $E$ ,  $Q$ ,  $f$ , and  $g_l$  is required. Only  $S$  is evaluated for each RGB value to be synthesized.

### 3.3 Extrapolation to unseen data

While our proposed conditional model generalizes well to unseen samples that are sufficiently similar to the training data and interpolation in latent space produces plausible textures, we find that extrapolation, the generalization performance to entirely new textures, leaves a lot to be desired. This is not surprising since generalization in the sense of extrapolation is a major unsolved problem for deep learning models. Nevertheless, supported implicitly by the architectural design of our texture sampler  $S$ , we propose an extrapolation strategy that significantly improves texture quality on exemplars not belonging to the training data manifold. Our method is a mixture between zero-shot learning and domain-adaption.

Given a new exemplar texture patch  $x$ , our idea is to fine-tune only a fraction of the parameters of our model in order to help improve the quality of generated samples. For this purpose we use  $E$  and  $Q$  to predict an initial guess for the latent code  $z$  and the transformations  $\{T_i\}$ . Next, we estimate a texture style  $w$  and from it a scale and bias vector  $\gamma, \delta$  for each hidden layer in  $S$ . In addition, we also predict the noise weight matrix  $A$  for the first four hidden layers in  $S$ . Finally, we perform stochastic gradient descent by evaluating random slices of the generated texture in each iteration. During this optimization we solely alter the parameters  $\theta = (T_i, \gamma_l, \delta_l, A_l)$ , with  $l$  being the layer index in  $S$ , while keeping all other parameters fixed. While also keeping the parameters in  $D$  fixed, we minimize  $\mathcal{L}_{\text{style}}$  for a few hundred iterations.

## 4 Experiments and results

In this section we evaluate the effect of the components of our framework by ablating them and we compare our system with a state of the art 3D texture synthesis method [5]. Note that all synthesized 2D images shown in this work are in fact slices in 3D. For more results and analysis, we refer the reader to the appendix.

Table 1: Quantitative comparison on the exemplars shown in Figure 3. We report SIFID  $\mu \pm \sigma$  ( $\times 10^5$ ) (lower is better).

	Henzler et al.	GAN + VGG	NI	$\alpha:1, \beta:0$	$\alpha:0, \beta:1$	$\alpha:0.1, \beta:1$
<i>wood</i>	0.67 $\pm 0.42$	0.19 $\pm 0.04$	0.28 $\pm 0.04$	0.29 $\pm 0.05$	<b>0.12</b> $\pm 0.02$	0.14 $\pm 0.02$
<i>granite</i>	0.53 $\pm 0.03$	0.31 $\pm 0.12$	0.34 $\pm 0.29$	0.28 $\pm 0.12$	0.43 $\pm 0.2$	<b>0.21</b> $\pm 0.10$

**Implementation details** We train all models using Adam optimizer [29] and we use (equalized [30]) learning rates of  $2 \times 10^{-3}$  for  $D$  and  $5 \times 10^{-4}$  for  $G$  ( $E$ ,  $Q$ , and  $S$ ). In each training iteration both  $G$  and  $D$  are updated once and sequentially. In  $\mathcal{L}_D$  we set  $\lambda = 10$ . An important factor is the choice of the hyperparameters  $\alpha$  and  $\beta$  in  $\mathcal{L}_G$ . Although various settings produce plausible outputs, we achieved best results when setting  $\alpha = 0.1$  and  $\beta = 1$ . Note that training a conditional model is not feasible unless  $\beta > 0$ . Setting  $\alpha = 0$  leads to perfectly stable adversarial training in both the single exemplar and the conditional setting, which we find a rather surprising insight. In the single exemplar setting we set  $n = 16$  and our conditional models use  $n = 32$  noise frequencies. We train on texture patches of size  $128^2$  and use noise instances of resolution  $64^{3n}$ .  $E$  maps texture patches to a latent representation of dimension 32. Our MLPs  $Q$ ,  $S$ , and  $f$  consist of 1, 5, and 1 hidden layers with 128 units each. We do not use any normalization layers, neither in MLPs nor in CNNs. During training, we sample completely random slices when training on isotropic materials (e.g. stone textures) by rotating a plane along all three axes. For more anisotropic structures like wood, we restrict random rotations along one axis, effectively minimizing the loss only along two axes and learning the third dimension implicitly. To efficiently compute texture values at many positions in a single forward pass, we implement  $S$  using  $1 \times 1$  convolutions. Training our model on a single exemplar takes a few hours on a single NVIDIA 2080ti GPU and learning an entire texture space takes up to several days depending on the dataset.

**Single exemplar** For efficiency, we perform many ablation studies in the single-exemplar setting. In order to draw robust conclusions we experimented with two very different exemplars: *wood* and *granite* (Figure 3 left). For comparisons we consider the following four variations of our framework: *GAN+VGG*: We replace our GramGAN style loss in  $\mathcal{L}_G$  with VGG style loss (similarly to [22–24]). *NI*, Noise-at-Input: Instead of injecting noise as in Section 3.1, we inject it at the input layer of  $S$ .  $\alpha:1, \beta:0$ : We use a vanilla WGAN loss without any style loss.  $\alpha:0, \beta:1$ : We solely optimize for GramGAN loss without traditional WGAN term.

In texture synthesis, the ground truth distribution is given by a single exemplar image and the quality of synthesized images is often evaluated by considering internal patch statistics. To quantitatively assess the differences between the approaches, we measure Single Image FID (SIFID) [16], a derivative of Fréchet Inception Distance (FID) [31] tailored to quantify the distance between internal patch statistics of two images. For each method we create 50 random 3D textures (using different random seeds) and from each texture we synthesize a randomly oriented 2D slice at the resolution of the ground truth exemplar. We then compute SIFID for each of the 50 resulting sample images and report their mean and standard deviation in Table 1, with qualitative examples shown in Figure 3.

The examples show that all variants of our approach are capable of reasonably reproducing the target texture. However, we achieve significantly more plausible results with our proposed method (last column in Figure 3). In addition, we also train the model by Henzler et al. [5] on both exemplars and find that it produces significantly lower-quality results (second column in Figure 3). The numbers in Table 1 confirm these findings. While the results suggest that  $\mathcal{L}_{\text{style}}$  is more important for the *wood* exemplar, WGAN loss is more effective on *granite*. However, note that solely optimizing for  $\mathcal{L}_{\text{style}}$ , i.e.  $\alpha:0, \beta:1$ , can cause artifacts that resemble Deep Dream [32] effects (tiny replicas of wood patterns when zoomed in Figure 3). For *NI* we use  $\alpha:0.1, \beta:1$  and for *GAN+VGG* we chose the hyperparameters to approximately result in the same weighting as ours with  $\alpha:0.1, \beta:1$ . Interestingly, we found that *NI* results in significantly less stable adversarial training and we had to lower the learning rate by a factor of 5 to  $1 \times 10^4$  to achieve convergence. In conclusion, using our GramGAN loss ( $\alpha:0.1, \beta:1$ ) yields consistently competitive results without any artifacts for the given substantially different exemplars.

We show additional qualitative examples of our model in Figure 1 and 4, including a comparison to [5] on actual 3D renderings using the synthesized textures as diffuse albedo. The comparison in

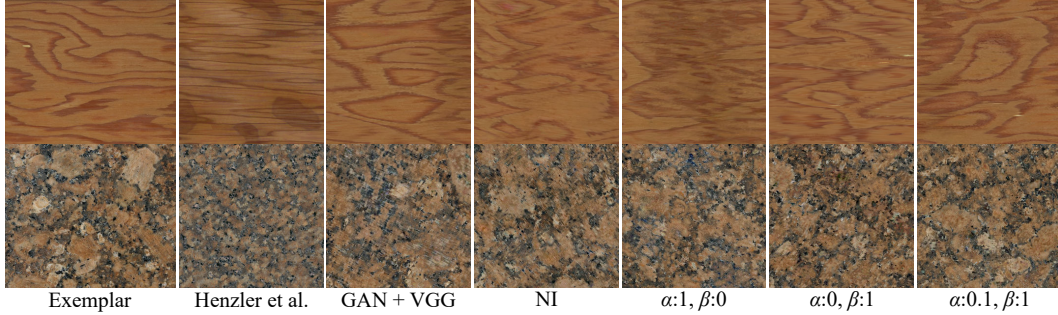


Figure 3: Qualitative comparison on two exemplars. Our approaches (3rd to last column) produce significantly better results than the model proposed by Henzler et al. [5]. Moreover, our final model (last column) achieves more realistic results than various variants of it (3rd to 6th column).



Figure 4: Qualitative comparison to Henzler et al. [5]. Left: exemplar. Middle: resynthesis Henzler et al. (top), ours (bottom). Right: 3D renderings Henzler et al. (left), ours (right).

Figure 4 shows that [5] produces implausible artifacts in 3D for anisotropic textures. This is a cause of sampling only axis-aligned slices during training, while we sample all possible slice orientations. The renderings are raytraced using *mitsuba renderer* [33] modified to perform inference on our model for texture look-ups. The *cube* model is rendered using perfectly diffuse albedo and light source, while the *sphere* model rendering features a more realistic scenario with a glossy coating material and an HDR environment map light source. The rendered images are high resolution, so please zoom in.

**Texture space** Next we report a quantitative evaluation of our conditional texture space model in comparison to the system proposed by Henzler et al. [5]. For this purpose we trained both models on a texture dataset consisting of 100 stone texture exemplars collected online. In this conditional setting, the input to both frameworks is an exemplar patch of resolution  $128^2$  and the systems learn to resynthesize the input texture. For evaluation we synthesized texture samples of size  $128^2$  from 22 reference input patches not seen during training, and measured their similarity to the references.

In Table 2 (first row) we report SIFID values averaged over the 22 samples generated by both frameworks. In addition, we also measured ground truth performance by sampling random crops from the respective training exemplars and compare them to the references. The numbers confirm that the outputs of our model are closer to the references in terms of SIFID. In addition, the comparison shows that SIFID for ground truth is not significantly lower. This can be explained by the fact that two random patches of the same texture exemplar image can look fairly different, especially for textures that feature very low-frequency variations. Note, however, that the computed SIFID numbers have rather high standard deviations due to the limited resolution of the texture images. In addition to SIFID we also measured average log-likelihood (ALL) reported in Table 2 (second row). An important property of generative models is to avoid producing artefacts and ALL has been proposed as a measure thereof [34], quantifying how probable generated samples are, given the ground truth density. ALL is typically estimated by using a Parzen window density estimate using a Gaussian kernel. Due to the stochastic nature of textures, we perform this evaluation over rather small kernel sizes to emphasize on the texture elements. In particular, we start with a large kernel size and reduce its size until there is a significant difference between the ALL of the methods. To set the second parameter, Gaussian kernel bandwidth, we performed a grid search using the ground truth test set. Our evaluation shows that our method is superior also in terms of ALL, although not as significant.

Finally, we conducted a formal user study to evaluate both the perceptual quality of the generated samples and their similarity to the reference. For this purpose participants were presented with a reference texture patch and three candidate patches: the ground truth patch, a patch generated by

Table 2: Quantitative evaluation of our framework in comparison to [5] and ground truth. We report  $\mu \pm \sigma$  for SIFID (lower is better), ALL (higher is better), and user study ranking (lower is better).

	Ground truth	Henzler et al.	GramGAN (ours)
SIFID $\times 10^5$	<b>2.46</b> $\pm 2.80$	2.60 $\pm 2.85$	2.47 $\pm 2.23$
ALL	<b>-294.85</b> $\pm 86.13$	-319.02 $\pm 70.61$	-317.23 $\pm 74.30$
rank from study	1.87 $\pm 0.85$	2.28 $\pm 0.71$	<b>1.85</b> $\pm 0.80$

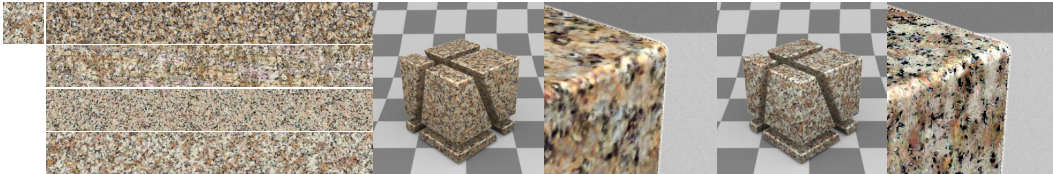


Figure 5: Qualitative results of conditional texture space model. Left: exemplar patch. Middle from top to bottom: Henzler et al., ours, ours extrapolated using VGG, ours extrapolated using  $D$ . Right: 3D renderings Henzler et al. (left) and ours (right), the latter looking more similar to the reference.

our model, and a patch produced by [5]. The participants were asked to rank these according to their *similarity* to the reference patch. For sake of clarity, we elaborated similarity as *how likely that the candidate is an image of the same material as in the reference image, e.g. perhaps a different region/section of the same sample*. The presentation order of textures and candidates were randomized for each participant. We received rankings from 21 participants for 22 texture references. We report the average ranks of 462 rankings per method in Table 2 (third row). A paired Wilcoxon signed rank test confirms that the users prefer our results over [5] (with  $p < 2 \times 10^{-11}$  at 5% significance level). Moreover, the difference between our results and ground truth is not statistically significant ( $p = 0.56$ ), whereas ground truth is significantly higher ranked than [5] ( $p < 1 \times 10^{-10}$ ). In Figure 4 we show a qualitative comparison of our texture space model on an exemplar texture patch with a texture significantly different than all training exemplars. This comparison shows that both [5] (first row) and our framework (second row) produce results fairly different from the input exemplar due to lacking extrapolation capabilities. Nevertheless, quantitative evaluation (SIFID over 50 random samples) indicate that our result ( $2.04 \pm 0.79$ ) is significantly closer to the reference than [5] ( $11.31 \pm 0.79$ ). Finally, we demonstrate that our extrapolation strategy proposed in Section 3.3 (forth row) further improves the output significantly ( $1.46 \pm 0.29$ ). We also show an alternative of our extrapolation strategy (third row) that minimizes  $\mathcal{L}_{\text{style}}$  using VGG instead of  $D$ . This experiment demonstrates that our discriminator features are much better suited than VGG features for style-based texture synthesis (SIFID:  $1.79 \pm 0.3$ ).

## 5 Conclusions

In this work we presented GramGAN, an novel framework for 3D texture synthesis from 2D exemplars. Key to our method is a novel loss function that combines ideas from GANs as well as style transfer, to optimally guide a synthesis model. We demonstrate that our model significantly outperforms state of the art, with superior results compared to existing alternatives. An interesting future direction would be to extend our framework to non-diffuse albedos including specular and normal maps by leveraging differentiable renderers.

## References

- [1] Ken Perlin. An image synthesizer. *ACM Comput. Graph. (SIGGRAPH)*, 19(3):287–296, 1985.
- [2] Ian Goodfellow, Jean Pouget-Abadie, Mehdi Mirza, Bing Xu, David Warde-Farley, Sherjil Ozair, Aaron Courville, and Yoshua Bengio. Generative adversarial nets. In *Advances in Neural Information Processing Systems (NIPS)*, pages 2672–2680, 2014.
- [3] Leon Gatys, Alexander S Ecker, and Matthias Bethge. Texture synthesis using convolutional neural networks. In *Advances in neural information processing systems (NIPS)*, pages 262–270, 2015.
- [4] Dmitry Ulyanov, Andrea Vedaldi, and Victor Lempitsky. Improved texture networks: Maximizing quality and diversity in feed-forward stylization and texture synthesis. In *IEEE Conf Computer Vision and Pattern Recognition (CVPR)*, pages 6924–6932, 2017.
- [5] Philipp Henzler, Niloy J Mitra, and Tobias Ritschel. Learning a neural 3D texture space from 2D exemplars. In *The IEEE Conference on Computer Vision and Pattern Recognition (CVPR)*, June 2020.
- [6] Alexei A. Efros and William T. Freeman. Image quilting for texture synthesis and transfer. In *ACM Comput. Graph. (SIGGRAPH)*, page 341–346, 2001.
- [7] Marcelo Bertalmio, Luminita Vese, Guillermo Sapiro, and Stanley Osher. Simultaneous structure and texture image inpainting. *IEEE Transactions on image processing*, 12(8):882–889, 2003.
- [8] Antonio Criminisi, Patrick Pérez, and Kentaro Toyama. Region filling and object removal by exemplar-based image inpainting. *IEEE Transactions on image processing*, 13(9):1200–1212, 2004.
- [9] Iddo Drori, Daniel Cohen-Or, and Hezy Yeshurun. Fragment-based image completion. *ACM Trans. Graph. (SIGGRAPH)*, 22(3):303–312, 2003.
- [10] Connelly Barnes, Eli Shechtman, Adam Finkelstein, and Dan B Goldman. PatchMatch: A randomized correspondence algorithm for structural image editing. In *ACM Transactions on Graphics (ToG)*, volume 28, page 24, 2009.
- [11] Soheil Darabi, Eli Shechtman, Connelly Barnes, Dan B Goldman, and Pradeep Sen. Image melding: combining inconsistent images using patch-based synthesis. *ACM Transactions on Graphics (ToG)*, 31(4):1–10, 2012.
- [12] Karen Simonyan and Andrew Zisserman. Very deep convolutional networks for large-scale image recognition. *arXiv preprint arXiv:1409.1556*, 2014.
- [13] Dmitry Ulyanov, Vadim Lebedev, Andrea Vedaldi, and Victor S Lempitsky. Texture networks: Feed-forward synthesis of textures and stylized images. In *ICML*, volume 1, page 4, 2016.
- [14] Justin Johnson, Alexandre Alahi, and Li Fei-Fei. Perceptual losses for real-time style transfer and super-resolution. In *European Conference on Computer Vision (ECCV)*, 2016.
- [15] Dmitry Ulyanov, Andrea Vedaldi, and Victor Lempitsky. Improved texture networks: Maximizing quality and diversity in feed-forward stylization and texture synthesis. In *IEEE Conf Computer Vision and Pattern Recognition (CVPR)*, pages 6924–6932, 2017.
- [16] Tamar Rott Shaham, Tali Dekel, and Tomer Michaeli. SinGAN: Learning a generative model from a single natural image. In *IEEE Int Conf Computer Vision (ICCV)*, pages 4570–4580, 2019.
- [17] Nikolay Jetchev, Urs Bergmann, and Roland Vollgraf. Texture synthesis with spatial generative adversarial networks. *arXiv preprint arXiv:1611.08207*, 2016.
- [18] Urs Bergmann, Nikolay Jetchev, and Roland Vollgraf. Learning texture manifolds with the periodic spatial GAN. In *Proceedings of the 34th International Conference on Machine Learning-Volume 70*, pages 469–477, 2017.

- [19] Anna Frühstück, Ibraheem Alhashim, and Peter Wonka. TileGAN: synthesis of large-scale non-homogeneous textures. *ACM Transactions on Graphics (TOG)*, 38(4):1–11, 2019.
- [20] Mehdi Mirza and Simon Osindero. Conditional generative adversarial nets. *arXiv preprint arXiv:1411.1784*, 2014.
- [21] Aibek Alanov, Max Kochurov, Denis Volkhonskiy, Daniil Yashkov, Evgeny Burnaev, and Dmitry Vetrov. User-controllable multi-texture synthesis with generative adversarial networks. *arXiv preprint arXiv:1904.04751*, 2019.
- [22] Wenqi Xian, Patsorn Sangkloy, Varun Agrawal, Amit Raj, Jingwan Lu, Chen Fang, Fisher Yu, and James Hays. TextureGAN: Controlling deep image synthesis with texture patches. In *IEEE Conf Computer Vision and Pattern Recognition (CVPR)*, pages 8456–8465, 2018.
- [23] Yang Zhou, Zhen Zhu, Xiang Bai, Dani Lischinski, Daniel Cohen-Or, and Hui Huang. Non-stationary texture synthesis by adversarial expansion. *arXiv preprint arXiv:1805.04487*, 2018.
- [24] Ning Yu, Connelly Barnes, Eli Shechtman, Sohrab Amirghodsi, and Michal Lukác. Texture mixer: A network for controllable synthesis and interpolation of texture. In *IEEE Conf Computer Vision and Pattern Recognition (CVPR)*, pages 12164–12173, 2019.
- [25] Tero Karras, Samuli Laine, and Timo Aila. A style-based generator architecture for generative adversarial networks. In *IEEE Conf Computer Vision and Pattern Recognition (CVPR)*, pages 4401–4410, 2019.
- [26] Ishaan Gulrajani, Faruk Ahmed, Martin Arjovsky, Vincent Dumoulin, and Aaron C Courville. Improved training of Wasserstein GANs. In *Advances in neural information processing systems (NIPS)*, pages 5767–5777, 2017.
- [27] Volodymyr Mnih, Nicolas Heess, Alex Graves, et al. Recurrent models of visual attention. In *Advances in neural information processing systems (NIPS)*, pages 2204–2212, 2014.
- [28] Xun Huang and Serge Belongie. Arbitrary style transfer in real-time with adaptive instance normalization. In *IEEE Int Conf Computer Vision (ICCV)*, pages 1501–1510, 2017.
- [29] Diederik P Kingma and Jimmy Ba. Adam: A method for stochastic optimization. *arXiv preprint arXiv:1412.6980*, 2014.
- [30] Tero Karras, Timo Aila, Samuli Laine, and Jaakko Lehtinen. Progressive growing of GANs for improved quality, stability, and variation. *arXiv preprint arXiv:1710.10196*, 2017.
- [31] Martin Heusel, Hubert Ramsauer, Thomas Unterthiner, Bernhard Nessler, and Sepp Hochreiter. GANs trained by a two time-scale update rule converge to a local nash equilibrium. In *Advances in neural information processing systems (NIPS)*, pages 6626–6637, 2017.
- [32] Alexander Mordvintsev, Christopher Olah, and Mike Tyka. Inceptionism: Going deeper into neural networks, 2015. URL <https://research.googleblog.com/2015/06/inceptionism-going-deeper-into-neural.html>.
- [33] Wenzel Jakob. Mitsuba renderer, 2010. <http://www.mitsuba-renderer.org>.
- [34] Olivier Breuleux, Yoshua Bengio, and Pascal Vincent. Unlearning for better mixing. *Universite de Montreal/DIRO*, 2010.

## A Appendix

Here we show additional results and analysis of our framework for 3D texture synthesis. We first demonstrate the capability of our system to learn a continuous latent texture space when trained on a dataset consisting of diverse textures (Section A.1). Next, we present more qualitative results that demonstrate the benefits of our approach compared to the system by Henzler et al. [5] (Section A.2). In Section A.3, we tabulate the network architectures of the convolutional neural networks used in our experiments. Finally, we present detailed results from our user study and all the images used therein in Section A.4.

## A.1 Latent space interpolation

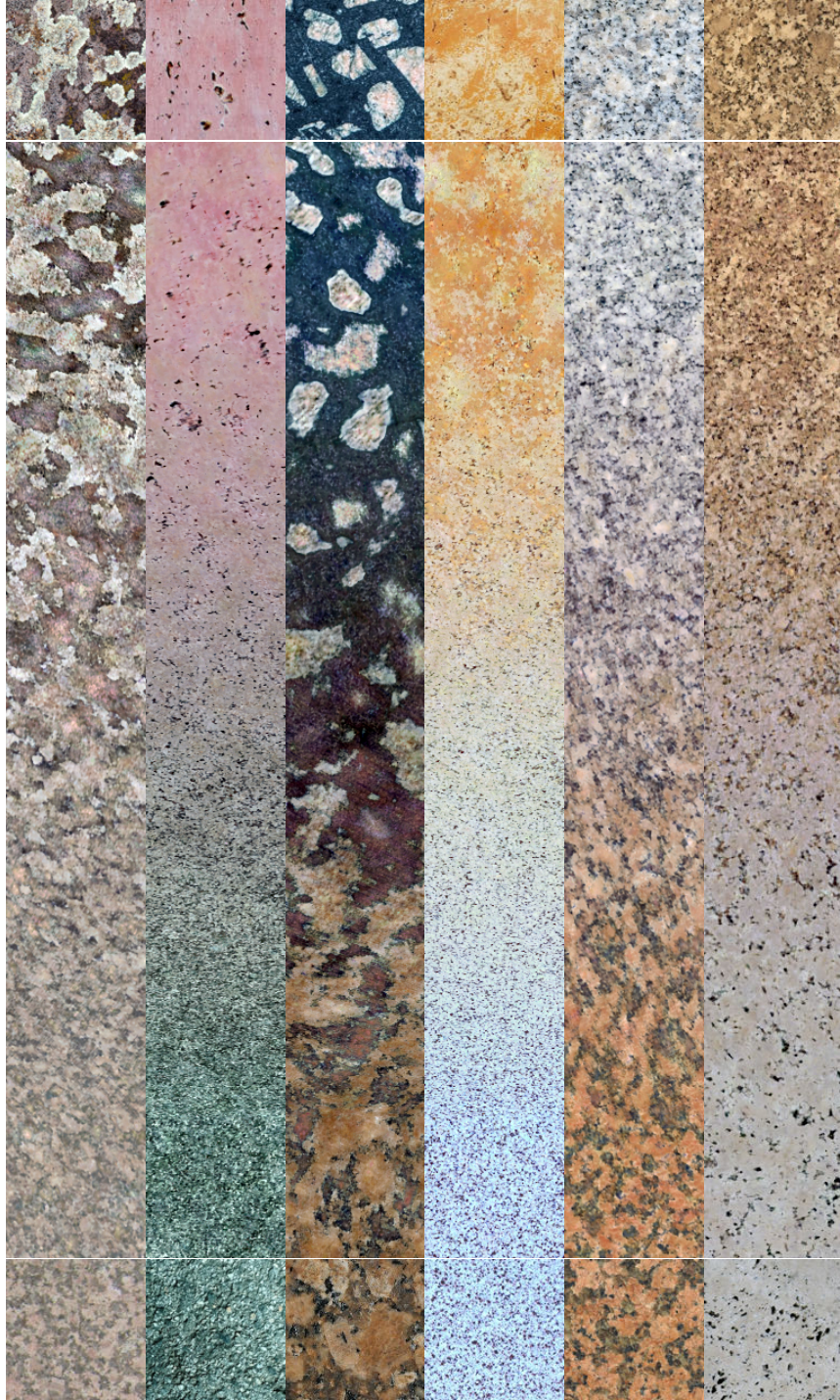


Figure 6: Linear interpolation in latent space  $z$ . Top: first exemplar. Bottom: second exemplar. Middle: interpolated result. First and last square in each strip correspond to resynthesized exemplars.

## A.2 Qualitative comparisons

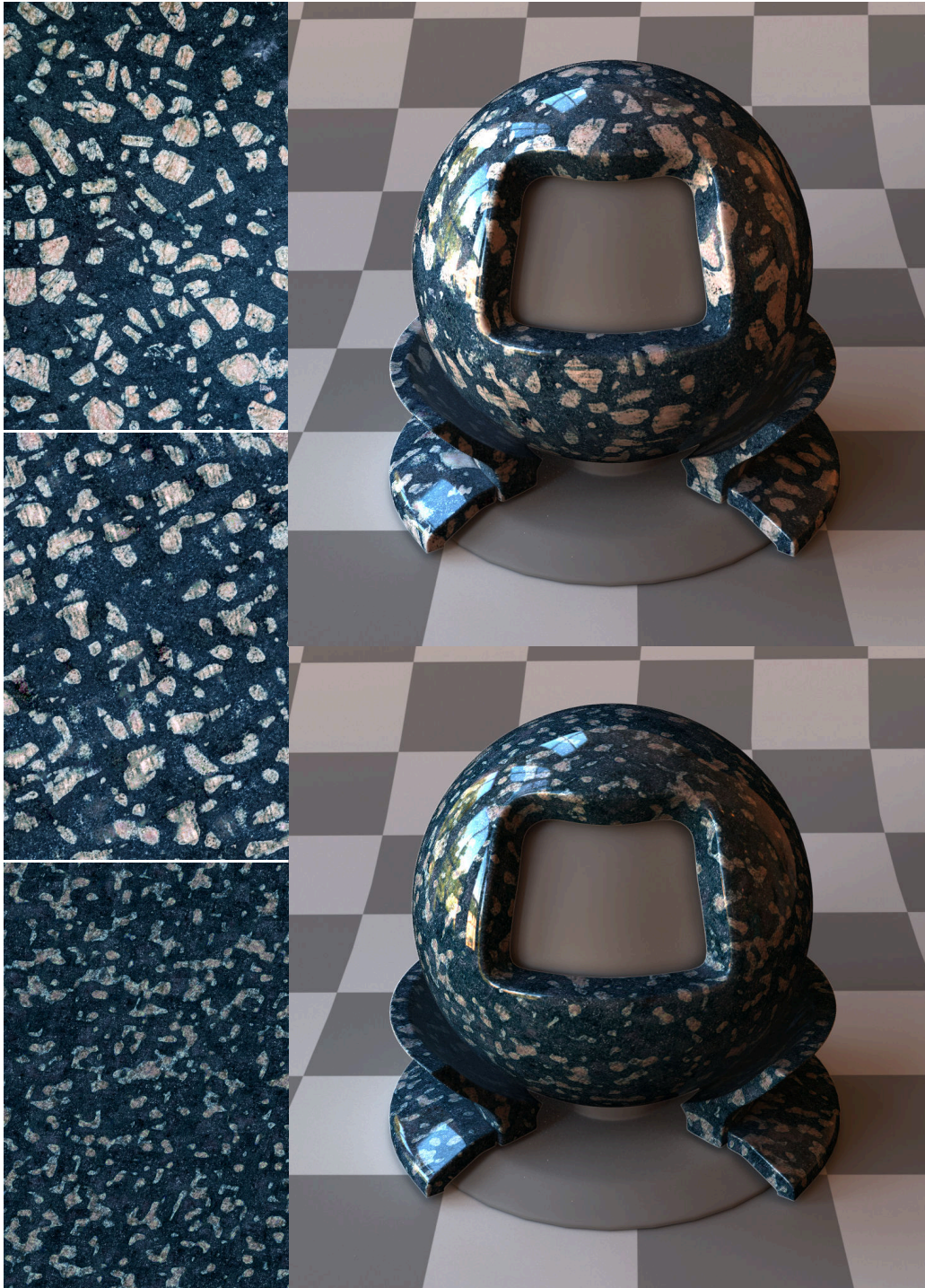


Figure 7: Single exemplar setting. Left: exemplar (top), ours (middle), Henzler et al. (bottom). Right: ours (top), Henzler et al. (bottom). Note how our result is closer to the exemplar texture.

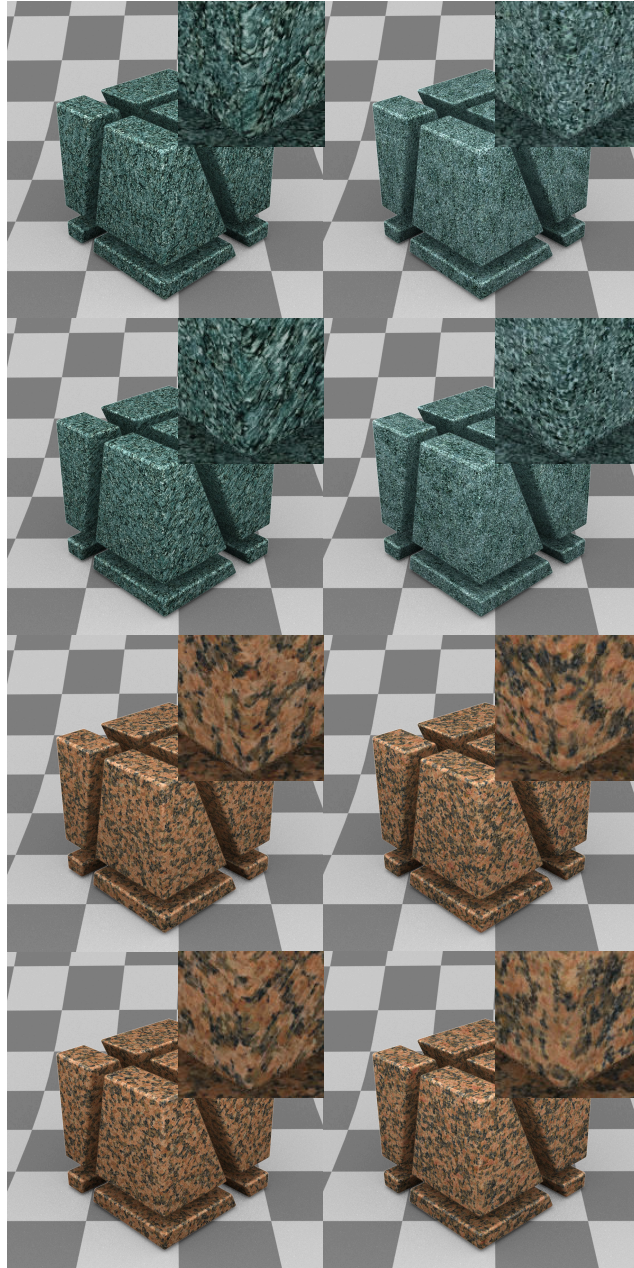


Figure 8: Texture space setting. Here we demonstrate artifacts that occur due to non-axis-aligned slicing. If only axis-aligned slices are sampled during training ([5]), distortion artifacts occur along non-axis-aligned slices. Left: Henzler et al. axis-aligned cube (first and third row) and  $45^\circ$  rotated cube (second and fourth row). Right: ours axis-aligned cube (first and third row) and  $45^\circ$  rotated cube (second and fourth row). Note how ours produces more consistent results for both axis-aligned and non-axis-aligned geometry. See Figure 10 (second row) and Figure 11 (third row) for exemplar images.

### A.3 Network architectures

Table 3: Network architecture of encoder  $E$ .

layer	activation	shape in	shape out	kernel
conv	LReLU	$128 \times 128 \times 3$	$128 \times 128 \times 32$	$3 \times 3$
pool	–	$128 \times 128 \times 32$	$64 \times 64 \times 32$	$2 \times 2$
conv	LReLU	$64 \times 64 \times 32$	$64 \times 64 \times 64$	$3 \times 3$
pool	–	$64 \times 64 \times 64$	$32 \times 32 \times 64$	$2 \times 2$
conv	LReLU	$32 \times 32 \times 64$	$32 \times 32 \times 128$	$3 \times 3$
pool	–	$32 \times 32 \times 128$	$16 \times 16 \times 128$	$2 \times 2$
conv	LReLU	$16 \times 16 \times 128$	$16 \times 16 \times 256$	$3 \times 3$
pool	–	$16 \times 16 \times 256$	$8 \times 8 \times 256$	$2 \times 2$
conv	LReLU	$8 \times 8 \times 256$	$8 \times 8 \times 256$	$3 \times 3$
pool	–	$8 \times 8 \times 256$	$4 \times 4 \times 256$	$2 \times 2$
conv	LReLU	$4 \times 4 \times 256$	$4 \times 4 \times 256$	$3 \times 3$
pool	–	$4 \times 4 \times 256$	$2 \times 2 \times 256$	$2 \times 2$
conv	LReLU	$2 \times 2 \times 256$	$2 \times 2 \times 256$	$2 \times 2$
pool	–	$2 \times 2 \times 256$	$1 \times 1 \times 256$	$2 \times 2$
dense	LReLU	256	256	–
dense	–	256	32	–

Table 4: Network architecture of discriminator  $D$ .

layer	activation	shape in	shape out	kernel
conv	LReLU	$128 \times 128 \times 3$	$128 \times 128 \times 32$	$3 \times 3$
conv	LReLU	$128 \times 128 \times 32$	$128 \times 128 \times 64$	$3 \times 3$
pool	–	$128 \times 128 \times 64$	$64 \times 64 \times 64$	$2 \times 2$
conv	LReLU	$64 \times 64 \times 64$	$64 \times 64 \times 64$	$3 \times 3$
conv	LReLU	$64 \times 64 \times 64$	$64 \times 64 \times 128$	$3 \times 3$
pool	–	$64 \times 64 \times 128$	$32 \times 32 \times 128$	$2 \times 2$
conv	LReLU	$32 \times 32 \times 128$	$32 \times 32 \times 128$	$3 \times 3$
pool	–	$32 \times 32 \times 128$	$16 \times 16 \times 128$	$2 \times 2$
conv	LReLU	$16 \times 16 \times 128$	$16 \times 16 \times 256$	$3 \times 3$
pool	–	$16 \times 16 \times 256$	$8 \times 8 \times 256$	$2 \times 2$
conv	LReLU	$8 \times 8 \times 256$	$8 \times 8 \times 256$	$3 \times 3$
pool	–	$8 \times 8 \times 256$	$4 \times 4 \times 256$	$2 \times 2$
conv	LReLU	$4 \times 4 \times 256$	$4 \times 4 \times 256$	$3 \times 3$
pool	–	$4 \times 4 \times 256$	$2 \times 2 \times 256$	$2 \times 2$
conv	LReLU	$2 \times 2 \times 256$	$2 \times 2 \times 256$	$2 \times 2$
pool	–	$2 \times 2 \times 256$	$1 \times 1 \times 256$	$2 \times 2$
dense	LReLU	256	512	–
dense	–	512	1	–

#### A.4 User study

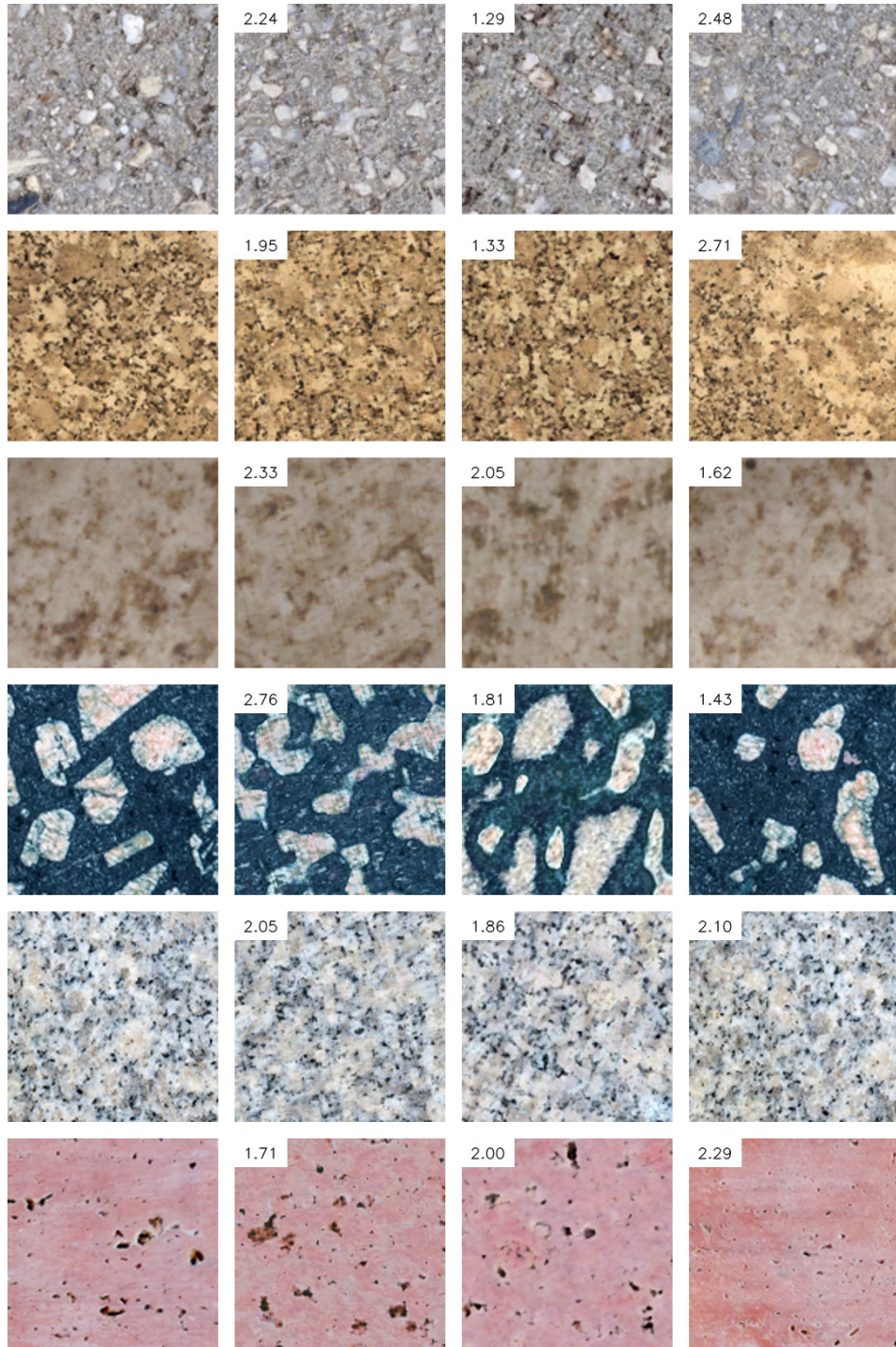


Figure 9: User study images palette 1. From left to right: reference, Henzler et al., ours, ground truth. Numbers show average user rank from our study (lower is better).

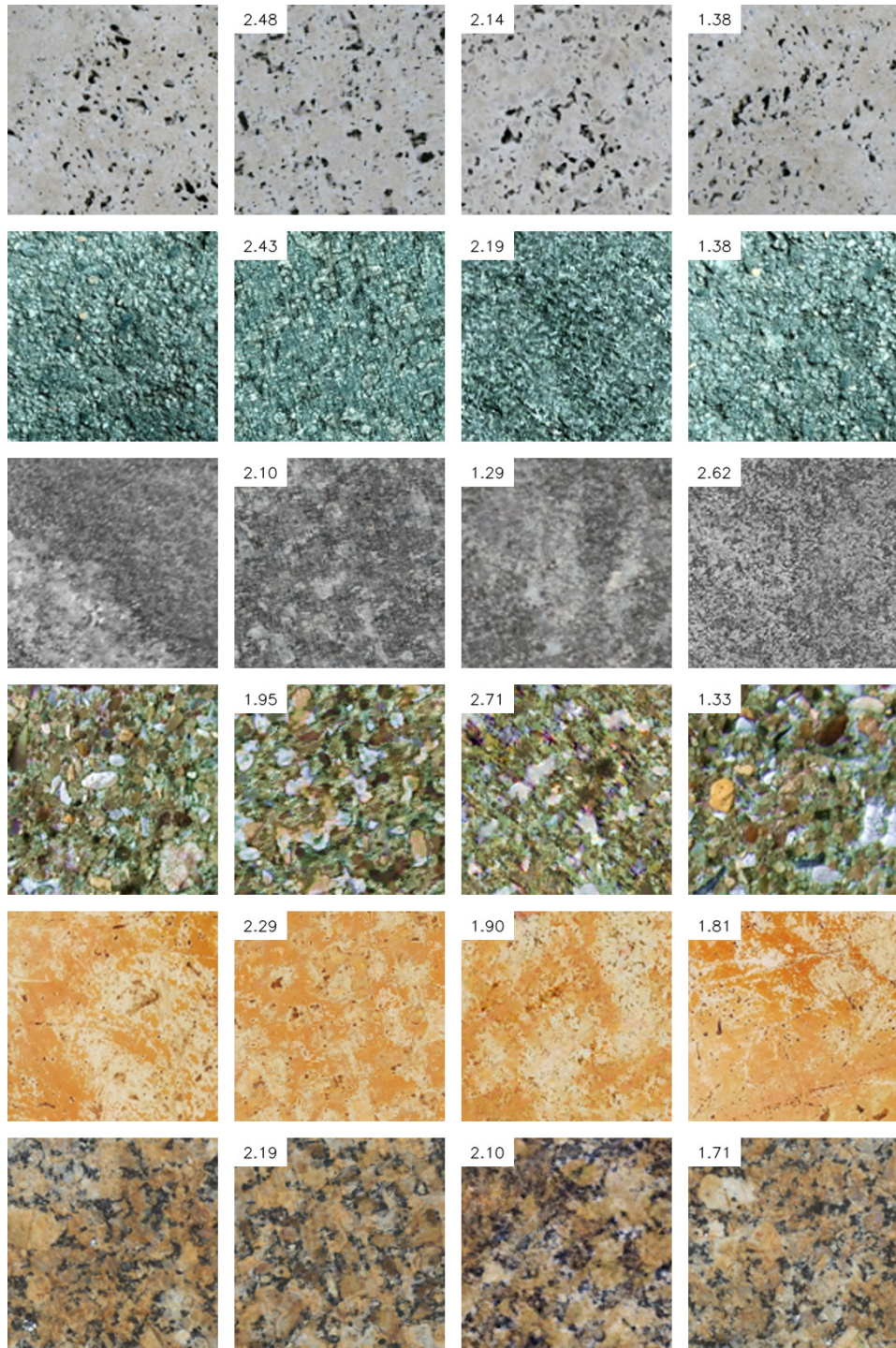


Figure 10: User study images palette 2. From left to right: reference, Henzler et al., ours, ground truth. Numbers show average user rank from our study (lower is better).

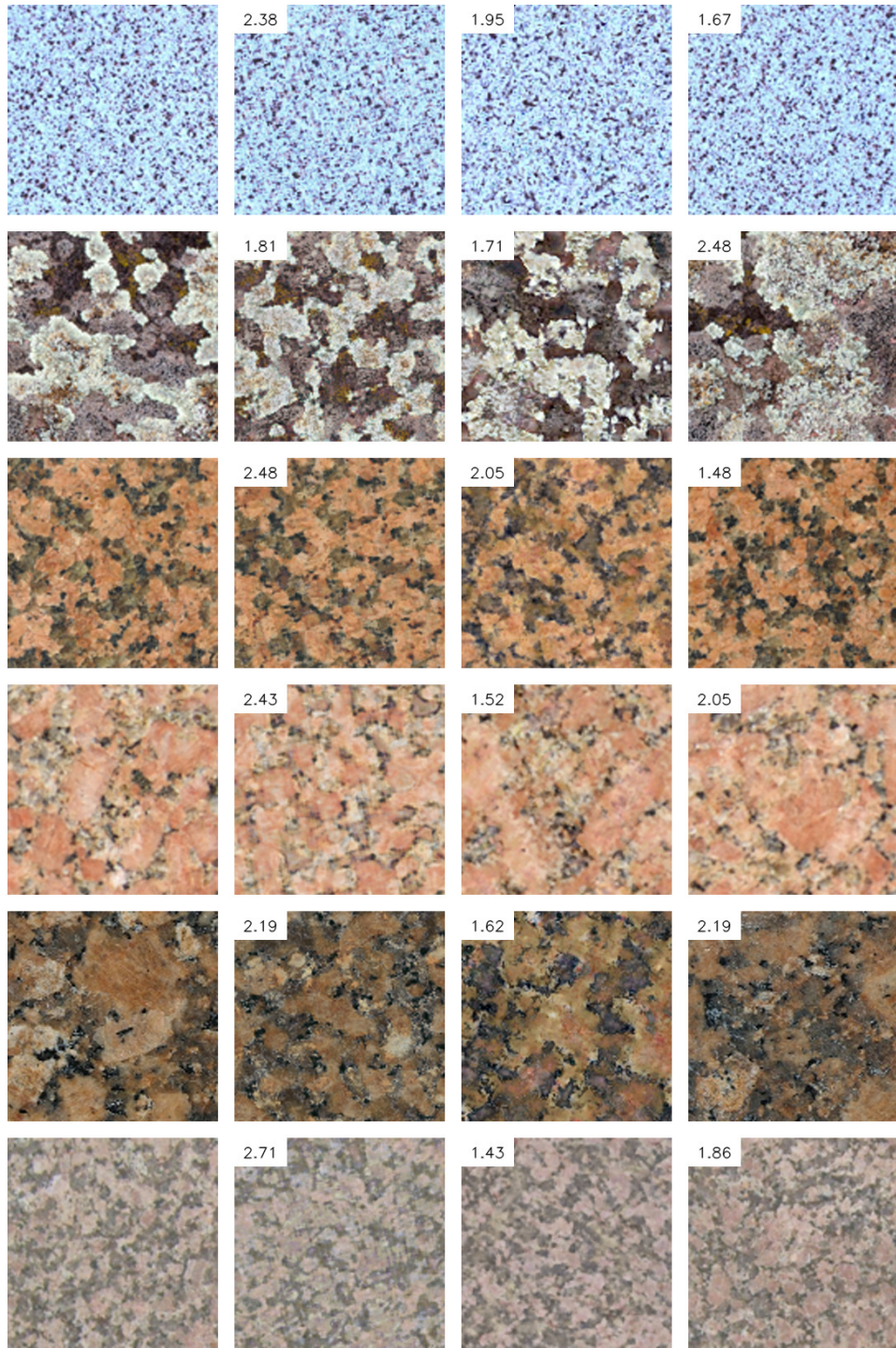


Figure 11: User study images palette 3. From left to right: reference, Henzler et al., ours, ground truth. Numbers show average user rank from our study (lower is better).

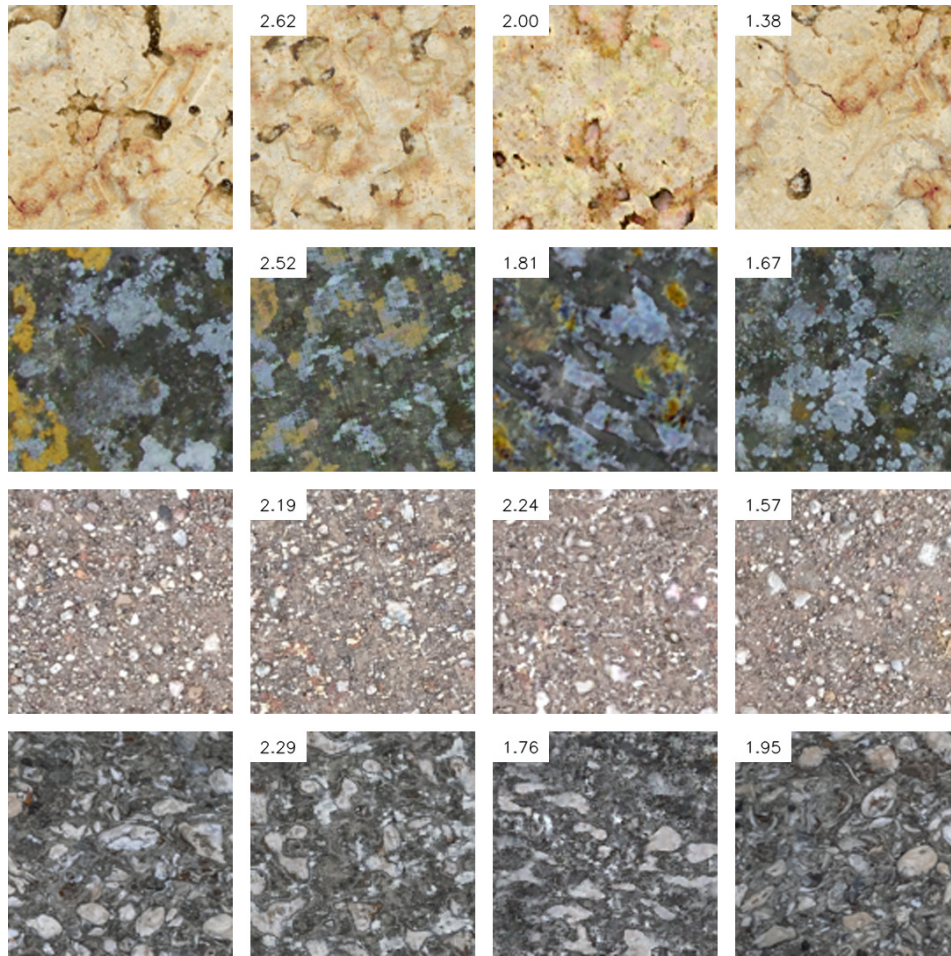


Figure 12: User study images palette 4. From left to right: reference, Henzler et al., ours, ground truth. Numbers show average user rank from our study (lower is better).